Soft Matter

PAPER

View Article Online
View Journal | View Issue

Cite this: *Soft Matter*, 2025, **21**, 1212

Lipophilic molecular rotor to assess the viscosity of oil core in nano-emulsion droplets†

Mohamed Elhassan,[ab] Carla Faivre,[ac] Halina Anton,[d] Guillaume Conzatti,[a] Pascal Didier,[d] Thierry Vandamme,[a] Alteyeb S. Elamin,[e] Mayeul Collot *[c] and Nicolas Anton *[a]

Characterization of nanoscale formulations is a continuous challenge. Size, morphology and surface properties are the most common characterizations. However, physicochemical properties inside the nanoparticles, like viscosity, cannot be directly measured. Herein, we propose an original approach to measuring dynamic viscosity using a lipidic molecular rotor solubilized in the core of nano-formulations. These molecules undergo conformational changes in response to viscosity variations, leading to observable changes in fluorescence intensity and lifetime, able to sense the volume properties of dispersed nano-domains. The lipophilic molecular rotor (BOPIDY derivatives) was specifically synthesized and characterized as oil viscosity sensing in large volumes. A second part of the study compares these results with rBDP-Toco in nano-emulsions. The objective is to evaluate the impact of the formulation, droplet size and composition on the viscosity of the droplet's core. The lipophilic rotor showed a universal behavior whatever the oil composition, giving a master curve. Applied to nano-formulations, it reveals the viscosity inside the nano-emulsion droplets, enabling the detection of slight variations between reference oil samples and the nano-formulated ones. This new tool opens the way to the fine characterization of complex colloids and multi-domain nano and micro systems, potentially applied to hybrid materials and biomaterials.

Received 21st October 2024,
Accepted 9th January 2025

DOI: 10.1039/d4sm01234h

rsc.li/soft-matter-journal

1. Introduction

Molecular rotors represent a particular category of viscosity-sensitive fluorescent compounds that serve as valuable probes for microenvironment characterization, particularly those which are inaccessible through conventional bulk rheological techniques.[1] The term ''molecular rotor'' refers to small synthetic fluorophores whose fluorescence emission is sensitive to the viscosity of the surrounding environment.[2] The sensing of the microenvironment has become an interesting research area since the local environment is the most relevant factor governing the physical and chemical behavior of surrounding molecules.[3] Fluorescence sensing techniques have played a crucial role in characterizing various properties such as viscosity, polarity, local acidity/basicity, pH, and temperature, thereby contributing to a more local understanding of properties.[4,5] Among various biophysical parameters, viscosity sensing plays an important role in many fields[6,7] including biological processes,[8] lipid bilayers,[9,10] and living cells.[11,12]

On the other hand, while measuring the rheological properties of a macroscopic sample is trivial, determining the micro-viscosity within micro/nano meter-sized objects remains extremely challenging.[13–15]

In literature reports,[16] an approach using cobalt ferrite nanoparticles (NPs) was described to sense the viscosity inside oil-in-water emulsions (coated with oleic acid) or in the continuous phase (coated with PEG), in order to compare with macroscale viscosity. In this case, NPs sizing around 14 nm were used and the micro-rheology obtained from the measurements of their magnetic susceptibility. A second literature example of particle tracking approach was described in a previous report,[17] using fluorescent beads of 0.75 μm. In conventional particle-tracking microrheology, the particle's motion is monitored, and the properties of the surroundings are obtained from the particle's trajectory. The mean-squared displacements of the beads were monitored as a function of the lag time, to obtain the diffusion coefficient, and deduce the medium viscosity. This is the

[a] *INSERM (French National Institute of Health and Medical Research), UMR 1260, Regenerative Nanomedicine (RNM), FMTS, Université de Strasbourg, F-67000 Strasbourg, France. E-mail: nanton@unistra.fr*
[b] *Department of Pharmaceutics, Faculty of Pharmacy, University of Gezira, Wad Medani 21111, Sudan*
[c] *Chemistry of Photoresponsive Systems, Laboratoire de Chémo-Biologie Synthétique et Thérapeutique (CBST) UMR 7199, CNRS, Université de Strasbourg, F-67400 Illkirch, France. E-mail: mayeul.collot@unistra.fr*
[d] *Laboratory of Biophotonic and Pathologies, CNRS UMR 7021, Université de Strasbourg, Faculté de Pharmacie, 74, Route du Rhin, 67401 Illkirch, France*
[e] *Omdurman Islamic University, faculty of pharmacy, department of pharmaceutics, Khartoum 00249, Sudan*

† Electronic supplementary information (ESI) available. See DOI: https://doi.org/10.1039/d4sm01234h

main difference between this particle-based approach and molecular rotors, for which viscosity is measured thanks to conformational changes.

Particle tracking is an attractive methodology that allows measuring physicochemical properties of dispersed systems. It is noteworthy that the particle-tracking method not only enables the measurement of viscosity but also allows the characterization of viscoelastic properties when external forces are applied to the particles, resulting in a specific response. This phenomenon is referred to as micro-viscoelasticity. However, a given scale of the particles is necessary to be sensitive to such external stimuli, in contrast to molecular rotors that cannot be sensitive to external stimuli. Consequently, molecular rotors can be used in a manner similar to the particle-tracking approach for studying dynamics in force-free environments. However, unlike particle tracking, molecular rotors can operate on a much smaller scale because of their significantly smaller size. Behind the fact that the microviscosity measurement by particle tracking needs specific experimental setup, the main limitation indeed lies in the scale range of the domains in which they allow to measure the viscosity. This scale range is, in the best condition, a few orders of magnitudes higher than the particles used, and finally limits micro domains to micrometer size, *i.e.* limited by the particle size. In contrast, molecular probes (like molecular rotors) do not have these limitations and allow measurements in domains with much lower scale, up to nano-domains. In that case, the typical length scale is also related to the diffusion distance of the probe over the measurement time, leading to an averaging of the sensed quantity over the probed volume at a small scale.

Other methods were reported in literature, nuclear magnetic resonance (NMR) and electron spin resonance (ESR) can be cited for studying the dynamics of confined molecules,[18,19] or also, the use of diffusing wave spectroscopy[20] which can be considered as an implemented dynamic light scattering. This approach allows assessing micro-rheology data from dispersed samples such as ageing, stability, and structural properties, complementarity with macro-rheology. Although this method is simple and efficient, it cannot be applied to study the internal properties of dispersed systems, especially at the nanoscale. We can finally cite another experimental setup based on colloidal-probe atomic force microscopy (AFM).[21] In that configuration, the micro-scale sample is set up between an oscillating tip and a support, to investigate the interfacial mechanics and dynamic rheological properties. The data collected are, to some extent, comparable to those obtained with macro-rheology. Here also, the main difference with the molecular probe is the scale of measurement (not transposable to nanoscale), and the additional constraint to confine the sample onto an AFM tip. These studies emphasize the need and interests in the development of new approaches to measure the fine physicochemical properties of dispersed micro- and nano-systems.

Molecular rotors offer a convenient means of measuring microviscosity by undergoing changes of intramolecular rotation and non-radiative relaxation, thus leading to observable changes in fluorescence intensity and lifetime. The rate of these conformational motions is directly influenced by viscosity. Therefore, variations in local viscosity induce significant changes in both fluorescence lifetime and fluorescence intensity.[22] Consequently, higher local viscosity restricts conformational changes of the molecular rotor, resulting in increased fluorescence lifetime and intensity. The fluorescence spectrum of a chromophore can be significantly dependent on its molecular environment, and thus on its interactions with the molecules around it. On the other hand, the study of fluorescence lifetime offers numerous advantages for assessing viscosity over fluorescence intensity; it is independent of the dye concentration. Also, it appears to be one of the most reliable and accurate methods for evaluating viscosity by using molecular rotors, eliminating potential experimental errors.[23–25] In addition, fluorescence lifetime detection can be integrated with imaging techniques like fluorescence lifetime imaging (FLIM).[26]

In this study, we used BODIPY-based molecular rotor to measure the microviscosity in the core of lipid nano-emulsions (NEs). NEs are lipid–oil droplets stabilized with surfactants, typically ranging in size from 20 to 300 nm.[27,28] Due to their stability and biocompatibility, NEs are emerging as promising carriers in various fields, including drug delivery, diagnostics, cosmetics, pesticides, and the food industry.[29–32] Compared to other nano-carriers, NEs have garnered attention as biomimicking ''green'' nanocarriers with significant potential for preparing contrast imaging agents and nanomedicines.[33] NEs have the distinct advantage of serving as liquid reservoirs for lipophilic active pharmaceutical ingredients (APIs) and/or lipophilic probes, dispersed in aqueous medium.[34,35] This characteristic allows NEs to encapsulate a large number of fluorescent dyes with reduced self-quenching, resulting in high quantum yield and ultrabright fluorescent nanomaterials. The brightness of these nano-droplets opens up new possibilities, such as single droplets tracking in cells or *in vivo* in small laboratory animals.[36–38] Herein, we formulated the nano-emulsions *via* spontaneous emulsification, a simple process widely described in the literature.[39,40] This method involves the formation of nanoscale droplets by mixing the oil and water phases, relying on the thermosensitivity of nonionic surfactants. As a result, a very homogeneous population of oil droplets, stabilized by the surfactant and dispersed in water, is formed.

To increase the encapsulation efficiency of fluorophores in NEs they should be highly soluble in oil to achieve high dye loading and sufficiently bulky to prevent aggregation-caused quenching (ACQ),[41] which would reduce the quantum yield of dyes encapsulated. Additionally, these dyes should be hydrophobic enough to remain within the NEs and photostable enough to enable tracking over time.[36] However, various parameters, such as hydrophobicity, polarity, composition, solubility, temperature, and viscosity, can significantly influence not only the physicochemical properties of the NEs but also the photophysical properties of the encapsulated fluorophores, leading to significant changes in the fluorescence properties of the NEs.[38,42] To date, the literature on nano-emulsions –and more generally on emulsions– considers that the oil core of formulated droplets conserves similar properties as the native

oil phase. This affirmation could, indeed, be considered as a corollary of the Bancroft's rule.[43,44] In general, the formulation of emulsions is considered producing oil droplets stabilized with a layer of stabilizers in the interfacial region. These amphiphiles molecules are soluble in the continuous phase, which determines the orientation of the interfacial curvature's concavity—directed toward the dispersed phase—and, consequently, the type of emulsion. This is finally why their interactions with the droplet composition are neglected.

Fluorogenic molecular rotors (FMRs) have demonstrated their efficiency in probing viscous environments through a correlation –power law– between fluorescence intensity, or lifetime, and viscosity. Green-emitting, and non-charged dyes known as 4,4-difluoro-4-bora-3a,4a-diaza-*s*-indacenes (BODIPYs) have become widely used in bioimaging. Indeed, these rotors serve to label proteins and DNA due to their high rotational ability and brightness.[45] This family of fluorescent probes is also used to characterize the modification of their solubilizing medium, as it is potentially linked to their fluorescence properties. However, understanding the relationship between the physicochemical properties of the environment in which the dyes are solubilized, the formulations, and the resulting fluorescence efficiency remains limited. To this end, we proposed to evaluate the relationship between the viscosity and fluorescence of rBDP-Toco, a derivative of BOPIDY, which is conjugated with α-tocopherol to enhance the rotor hydrophobicity,[46] and allowing an efficient solubilization in oils (see details on the chemical synthesis in Section 1 of ESI†). This BODIPY rotor moiety used in this study is a golden standard and was abundantly characterized in the literature, notably by the group of Kuimova *et al.*,[1] and was also applied to bioimaging in previous reports.[47,48] The advantage of this BODIPY rotor is its high sensitivity toward variations of viscosity notably using fluorescence lifetime and its low sensitivity toward other environmental changes like temperature[49] or polarity.[50] At this point, an important remark on the use of molecular rotors should be made: in homogeneous systems, the viscosity measured by rotors is typically related to macroscopic measurements through a calibration curve. However, in some cases, such as polymer solutions, this relationship may not hold. For instance, rotors may sense only the solvent viscosity, while macroscopic viscosity reflects the entire system, as demonstrated in previous studies.[51,52] In contrast, in homogeneous systems like those examined in the current study, the viscosity measured by the rotor is generally well correlated with macroscopic viscosity, as has been widely demonstrated in aqueous media.[47]

In the present study, we render the well-known molecular rotor lipophilic by coupling it with a lipid moiety (tocopherol), as illustrated below (Scheme 1) that presents the nano-emulsion formulation. We have previously shown that, when coupled to BODIPY, tocopherol drastically enhanced the BODIPY solubility.[46] This coupling does not affect the viscosity sensitivity, nor it modifies the fluorophore structure. In addition, it is important to note that this lipophilic BODIPY molecular rotor is recognized to have a very weak sensitivity to solvent polarity, as described in previous studies.[50]

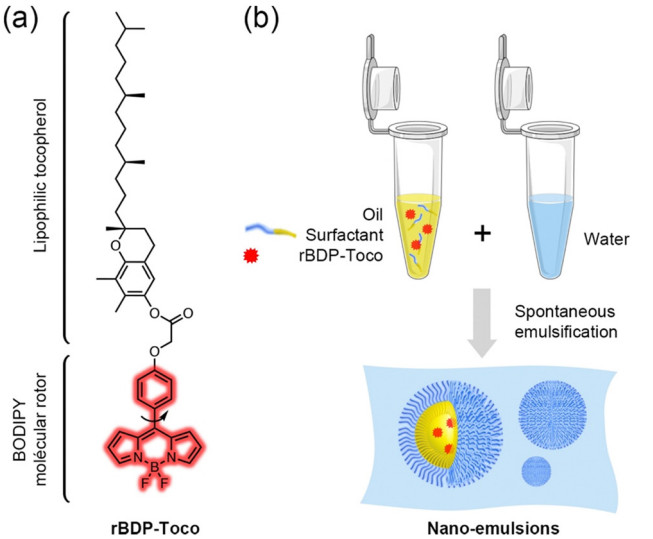

Scheme 1 (a) Structure of rBDP-Toco. The viscosity fluorescent reporter is a BODIPY molecular rotor, the lipophilicity was enhanced by coupling with the lipid tocopherol. (b) Principle of the nano-emulsion formulation by spontaneous emulsification.

The first part of this study focuses on characterizing the lipophilic molecular rotor, in order to establish the correlation between the actual viscosity of the oily phase of pure oil mixtures and optical properties. The second part is dedicated to the characterization of the oil properties when in nano-formulation by comparing the actual microviscosity with the viscosity of the oil core. In the literature, such molecular rotors have been used as probes in other types of applications, such as plasma membrane viscosity[53] or cell viscosity.[54] Here, we originally focus on sensing nanoscale oil domains and investigating the links between nano-emulsion properties and rotor response. We highlight that there can be significant differences between fluorescence characterization, which is commonly used in nano-emulsion studies, and fluorescence lifetime measurements, which primarily focus on molecular behavior without considering concentration effects. However, the simultaneous influence of temperature on viscosity and the photophysical behavior of fluorophores is often overlooked.[55] Nevertheless, temperature variations can introduce significant offset in viscosity readouts, and *vice versa*. Therefore, the final part of this study investigates the effect of temperature on the photophysical behavior of rBDP-Toco.

To conclude, this study proposes a new approach to sense the properties of nanoscale formulation, and potentially applicable to a broad range of materials, nanomaterials and multi-scale materials in general. For this reason, it presents a high potential in the characterization of colloids, and in the understanding of their behavior and composition.

2. Materials and methods

2.1. Materials

The oil phase, vitamin E acetate (VEA), was provided by Tokyo Chemical Industry (Tokyo, Japan), castor oil from Sigma-Aldrich

(France), and Labrafac WL 1349 (medium chain triglycerides, MCT) was obtained from Gattefossé (Saint-Priest, France). The nonionic surfactant used, Kolliphor® ELP was purchased from BASF (Ludwigshafen, Germany). A stock solution of 4.3 mM of the rBDP-Toco dye in dioxane was prepared beforehand (structure of rBDP-Toco is reported in Scheme 1(a)). Milli-Q water was obtained from a Millipore filtration system and used in all experiments. All chemicals were of analytical grade. rBDP-Toco was synthesized, the protocols and characterizations can be found in the ESI.†

2.2. Methods

2.2.1. Preparation of the oils mixture. In order to prepare oils possessing increasing viscosities, highly viscous oils (VEA and castor oil) were mixed at various ratios with lower viscosity MCT, thus we prepared: (i) MCT/castor oil and (ii) MCT/VEA. The oil mixture was homogenized at 80 °C in a thermomixer (Eppendorf) for 5 minutes, and then vortexed for 5 minutes. The different oil ratios were gradually modified, as described in the Section 3.1 below, with a ratio of the more viscous oil varying from 0 wt% wt to 100 wt%.

2.2.2. Rheological characterization. Rheology was performed on a HAAKE MARS 40 Rheometer (Thermo Scientific) using geometries of 35 mm diameter parallel plates with a gap of 0.1 mm. The volume of the oil sample (0.1 mL) was added to the plate geometry, and the temperature was set at 20 °C. The rotational rheometer was in controlled rate mode for which a shear rate ($\dot{\gamma}$) was applied and shear stress measured. The applied range of shear rate $\dot{\gamma}$ was from 0.1 to 1000 s^{-1}. All the measurements were performed in triplicate.

2.2.3. Absorption and fluorescence spectra. Absorbance and fluorescence spectra of oil mixtures were performed with a Thermo Scientific™ Varioskan™ LUX multimode microplate reader. The absorption spectra were scanned from 300 to 700 nm, while the emission spectra were recorded from 478 to 700 nm with an excitation wavelength of 460 nm. The sample prepared for analysis was a mixture of 4.6 μL of the rBDP-Toco dye (of stock solution at 4.3 mM in dioxane) and 1995.4 μL of oil. Then, 150 μL of the prepared sample was analyzed. Transparent microplates were used for absorbance spectra analysis and black microplates for fluorescence analysis. Fluorescence intensities of nano-emulsions were measured according to the same methodology, and, in order to compare their values, fluorescence intensity (FI) is normalized with oil amount as reference (as oil amounts can vary between the different formulations and pure oil mixtures). All the measurements were performed in triplicate.

2.2.4. Fluorescence lifetime measurements. Time-resolved fluorescence measurements were performed with the time-correlated single-photon counting technique with excitation at 500 nm (supercontinuum laser NKT Photonics SuperK Extreme with 10 MHz repetition rate). Samples are set up in a classic quartz 1 mL cuvette. The fluorescence signal was collected at 515 nm using a polarizer set at magic angle and a 16 mm band-pass monochromator (Jobin Yvon). The single-photon events were detected with a micro-channel plate photomultiplier R3809U Hamamatsu, coupled with a pulse preamplifier HFAC (Becker-Hickl GmbH) and recorded on a time-correlated single photon counting board SPC-130 (Becker-Hickl GmbH). Time-resolved exponential decays were fitted by using an exponential function convolved with a normalized Gaussian curve of standard deviation σ standing for the temporal instrument response function (IRF) and a Heavyside function. The fitting function was built in Igor Pro (Wavemetrics). All emission decays were fitted using a weighting that corresponds to the standard deviation of the photon number squared root. The lifetimes were measured for the pure oil mixtures (castor oil/MCT and VEA/MCT mixtures) with different viscosities to establish the calibration of the molecular rotors with actual macroscopic viscosity obtained with the oscillatory rheometer.

2.2.5. Formulation of nano-emulsions. Nano-emulsions (NEs) were formulated by the spontaneous emulsification method. As illustrated in Scheme 1(b), the first phase of {oil + nonionic surfactants} is heated and homogenized, and then suddenly mixed with aqueous phase (MilliQ water) at 80 °C. As a result, the oil phase is broken up and generates oil-in-water nano-emulsion droplets.[56] Loading such nano-emulsion with a dye only consists in solubilizing the probe in the oil phase and follow the same formulation process, without impact on the droplet's properties. The proportions with the nonionic surfactant Kolliphor ELP® were defined as surfactant-to-oil weight ratio (SOR), defined as SOR = $100 \times w_{surfactant}/(w_{surfactant} + w_{oil})$,[57] where w is the weight of the different compounds, varied from 50% to 70%. The amount of water phase is added to achieve 80 wt% water in the final suspension. It is worth noting that the nano-emulsion formulation process by spontaneous emulsification is a robust process, unaffected by slight modifications in the oil composition or by the solubilization of compounds in the oil (to a certain extent).[36] Thus, the formulation of nano-emulsions with and without rBDP-Toco at 4.3 mM does not affect the formulation process and droplet size.

2.2.6. Characterizing nanodroplet size distribution. The droplet size distribution, mean apparent hydrodynamic diameter, and polydispersity indexes (PDIs) were determined by dynamic light scattering (DLS)[58] using Malvern® Nano ZS instrument (Malvern, Orsay, France). The nano-emulsion samples were diluted 10 times in distilled water. Size distribution and PDI were recorded at a temperature of 25 °C. All the measurements were performed in triplicate.

2.2.7. Statistical analysis. All quantitative data are expressed as mean values plus or minus the standard deviation calculated from three independent experiments.

3. Results and discussion

3.1. Rheological characterization

Dynamic viscosities (η) are represented against shear rate $\dot{\gamma}$, and report in ESI† (Fig. S1) for the different oil mixtures. Viscosity η shows a gradual decrease and plateau stabilization, which is actually a phenomenon known for lower values of shear rates with lower intermolecular interactions,[59] and stabilize at higher values of shear rates to a Newtonian behavior. It is worth noting

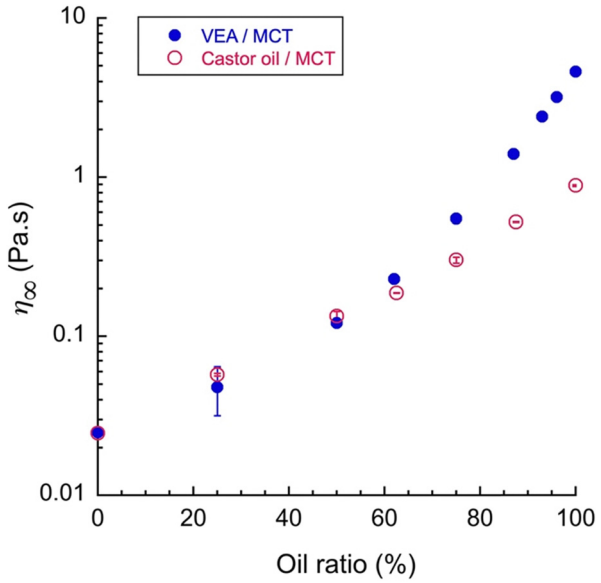

Fig. 1 Dynamic viscosities of oil mixtures. VEA or castor oil concentration (%) mixed with MCT.

that measuring the zero-shear viscosity using a plate-plate geometry is challenging due to limitations at low shear rates. Utilizing viscosity values from the Newtonian plateau observed at higher shear rates provides a viable alternative. We propose retaining the values from the Newtonian-like region, keeping in mind that we do not measure the zero-shear viscosity with the rheometer. Therefore, our objective is to present a correlation between this macroscopic behavior and the zero-shear results obtained from molecular rotor measurements in order to characterize the rBDP-Toco properties. Accordingly, we collect the values of stabilized viscosities in the plateau region (η_∞), which are reported in Fig. 1, for the two oil mixtures. The number of measurements was adapted to the oil mixtures, with a higher number for VEA/MCT mixture since the curve underwent a higher variation in the 80–100% range.

For pure MCT, η_∞ tends to (24.0 ± 0.1) mPa s, and the two curves are superimposed up to about 60%, then show a drastic separation that allows a significant difference in the properties of the two oil mixtures.

3.2. Fluorescence characterization of rBDP-Toco

The molecular rotor rBDP-Toco is dissolved in the different oil mixtures, and its fluorescence properties are subsequently characterized (see the spectral characterization in ESI,† Section 3). Once excited at 460 nm, FI are measured as the maximum intensity of the peak at 512 nm, and their values are reported in Fig. 2(a) in function of the oil composition (oil ratio of VAE and castor oil in MCT), and in Fig. 2(b) as a function of their viscosities obtained from Fig. 1.

Fig. 2(a) shows first the correlation between FI of rBDP-Toco, with the viscosity of its solubilizing medium. As the viscosity of the medium increases, the fluorescence intensity of the fluorogenic molecular rotor increases. This can be explained by the restriction of intramolecular rotation

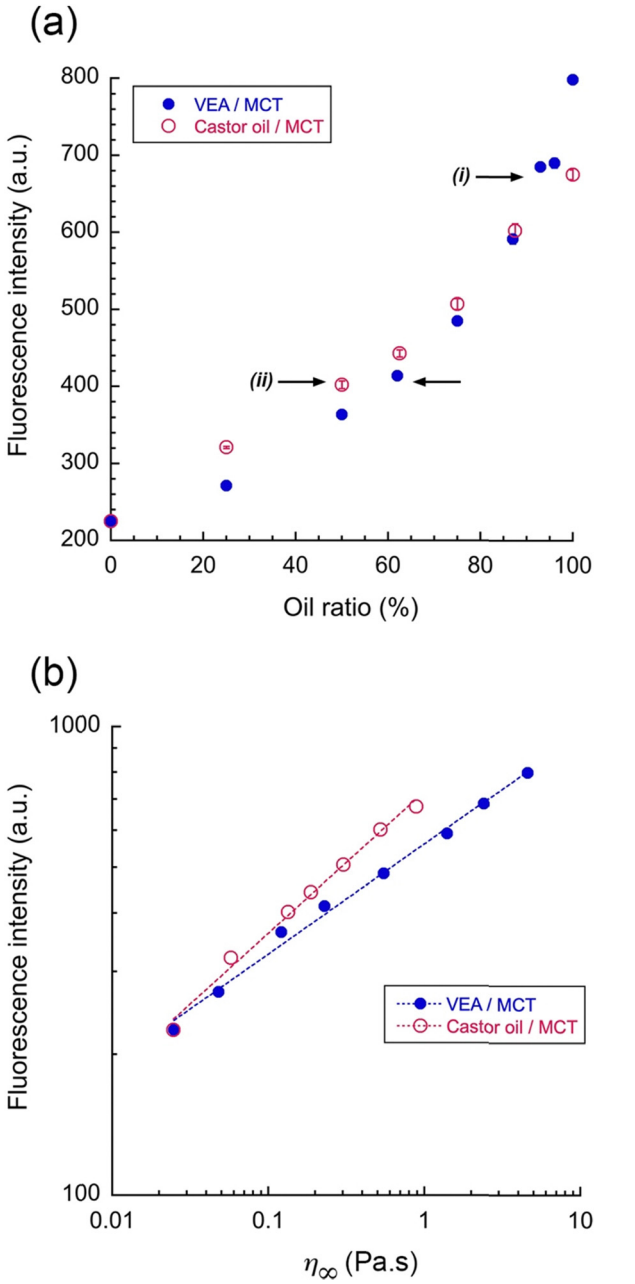

Fig. 2 Fluorescence intensity (λ_{ex} = 460 nm, λ_{em} = 512 nm) of rBDP-Toco dissolved in different oil mixtures, represented (a) against VEA or castor oil concentration (%) mixed with MCT, and (b) against the corresponding viscosities of these oil mixtures (obtained from Fig. 1).

commonly observed in fluorophores with the structure of molecular rotors, a phenomenon known as ''motion-induced change in emission''.

On the other hand, Fig. 2(a) compared oil mixtures with different viscosities and reveals very similar FI values –whereas clear difference has been expected. When FI values are transposed in function of η_∞, in Fig. 2(b), two distinct curves are shown, described by power laws. It follows therefore that rBDP-Toco has a clear response to a viscosity rise, but the efficiency of this response depends on the nature of oil.

These first results emphasize significantly different fluorescent behavior of rBDP-Toco in function of its solubilization medium, and thus the limitation of this approach to be considered as a universal viscosity probe. This result is likely due to the slightly different efficiency of these oils to solubilize such a molecular rotor, which can result in slight differences in the actual dye concentrations in oil.

Consequently, fluorescence lifetimes (τ) were measured for all these samples. The main difference from the simple fluorescence intensity is that lifetime measurement is not sensitive to concentration or related solubility issues. Results are reported in Fig. 3, and as opposed to those of FI, the fluorescence lifetime appears independent of the oil's composition and the two oil mixtures show results that can be superimposed.

This result is important and shows the potential of such molecular rotors as viscosity probe independently to the nature of the oil. When fluorescence characterization is classically associated with the measurements of FI, thus we can consider τ here as the reference. However, comparing lifetime and FI remains interesting to refine the characterization of the probe in its solubilizing medium: in the present case, rBDP-Toco appears more soluble in MCT/castor oil mixtures compared to MCT/VEA ones. This behavior is generally modeled with the Förster–Hoffmann power law,[60]

$$\tau = C \times (\eta_\infty)^x$$

where C is a constant and x represents the sensitivity of the molecular rotor towards viscosity. The fit gives C = 3.96 and x = 0.20 provided that shear stress is expressed in Pa and viscosity is expressed in Pa s. This model can be phenomenologically justified by considering a theory based on the concept of free volume.[61]

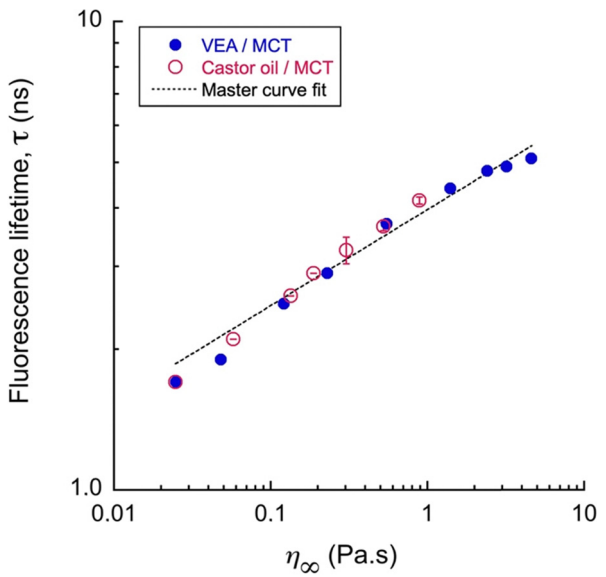

Fig. 3 Fluorescence lifetime (λ_{ex} = 460 nm, λ_{em} = 512 nm) of rBDP-Toco dissolved in different oil mixtures, represented against viscosities of oil mixtures of VEA or castor oil concentration (%) mixed with MCT.

A complementary set of experiments was undertaken, to investigate the effect of temperature on the behavior of rBDP-Toco dye, and reported in ESI† as Fig. S2. Viscosity and τ were measured for VEA/mixture over a temperature range from 20 °C to 55 °C, (Fig. S2(a) and (b), ESI†) for representative ratio (VEA ratio from 75% to 100%) and represented together (Fig. S2(c), ESI†). This analysis showed that the lifetime recorded at the same temperature did not overlap, and as well, were not superimposing with the master curve at 20 °C. As the calibration curve fit represents a generalized behavior derived from various calibration curves and systems with differing compositions, we refer to it as the "master curve" in this discussion.

This finding suggests that the behavior of the molecular rotor is strongly dependent on the temperature and does not allow comparing different compositions at different temperatures. Fig. S2(c) (ESI†) confirms that changing the study temperature would alter the master curve, the complex interplay between these factors, and emphasizes the importance of considering both viscosity and temperature effects in studying such systems. In summary, it appears that, at a given temperature, molecular rotors are accurate viscosity sensors, for different types of lipophilic phases, and can even reveal slight variations in their composition. Changing the temperature affects viscosity and the dye microenvironment properties. Since the lifetime-viscosity calibration curve varies with temperature, a new calibration is required for each temperature. This highlights that molecular rotor-based viscosity measurements are reliable only at a constant temperature.

3.3. Measuring the microviscosity in nano-emulsions

3.3.1. Effect of oil type on the size distribution of nano-emulsions. In order to understand the properties of nano-emulsions and the impact of the nanoscale formulation on the oil core of the droplets, we formulated the aforementioned different oil mixtures as nano-emulsions. The properties of nano-emulsions –*i.e.* size and dispersity– formulated by spontaneous method depend on the nature of the oil and the amount of surfactant used. The nano-droplet size decreases as the surfactant amount increases.[40] Nano-emulsification occurs in a specific condition when oil, surfactant and water are mixed together, as widely described.[27]

The efficiency of the spontaneous emulsification process depends on the relative affinities of the surfactants, with oil, and water, and thus slightly differs when using different oils. In this study, we have selected three different surfactant amounts (SOR = 50%, 60% and 70%) and monitored the size and polydispersity for the two oil mixtures (castor oil/MCT and VEA/MCT). The results are reported in Fig. 4 and emphasize the respective effects of the different oils in the droplet's size.

Representative size distributions are reported in the ESI† section, Fig. S3. The most efficient process (*i.e.*, the process that gives the smaller droplets) arises when using VEA, giving sizes below 50 nm. Then, MCT and castor oil gives droplets sizes around 100 nm and 130 nm, respectively (Fig. 4(a) and (b)). The PDI values (Fig. 4(c) and (d)) are below 0.3, and show a good

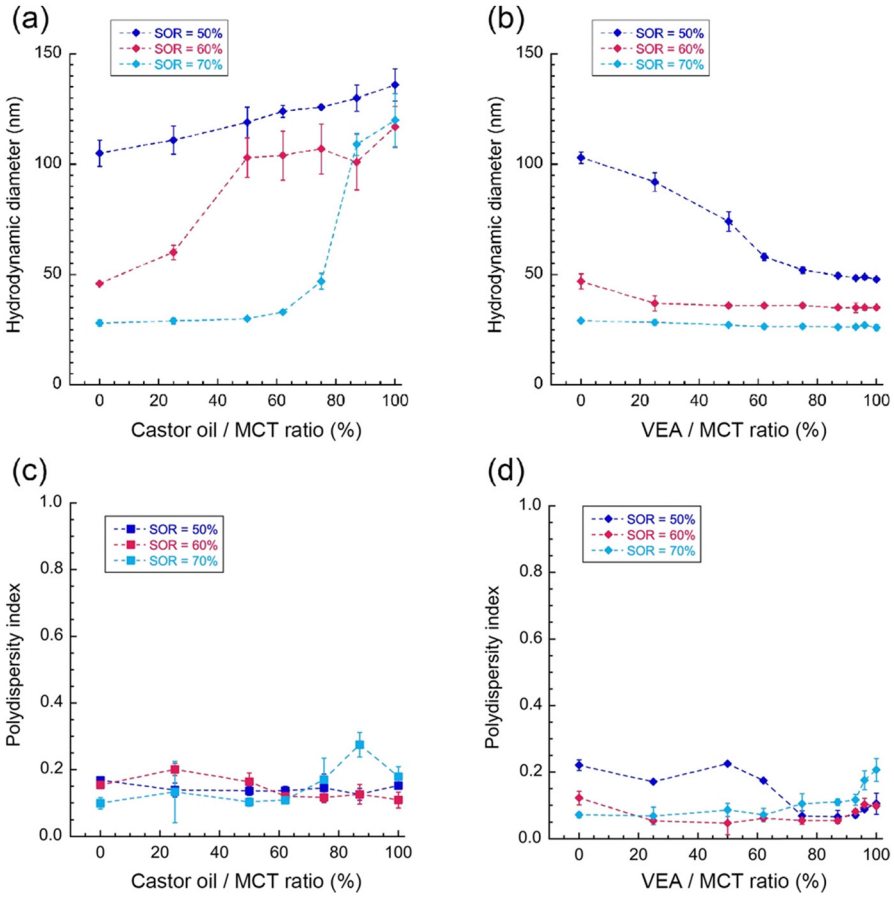

Fig. 4 Nano-emulsion characterization. Apparent hydrodynamic diameter (a) and (b), and corresponding PDI (c) and (d), for the different oil mixtures, for three surfactant amounts.

monodispersity of the droplet population and validate the size results.

These variations are due to the difference between surfactant affinities for these various oils, which could modify the mobility of surfactants and water in the {oil + surfactant} phase. This results in the spinodal decomposition of the oil phase, which turns into nano-droplets.[62] This behavior was also reported with change in the oil composition or oil chemical structures.[46,63–65] Interestingly, despite variations in the viscosities of these oils, no clear correlation between viscosity and the results depicted in Fig. 4 is apparent. Even, there is no correlation between viscosity and droplet size: the more viscous oil VEA gives smallest sizes, while the MCT showing the lowest viscosity gives droplets sizes between VEA and castor oil. Previous research has provided conflicting findings regarding the influence of oil phase properties on the formation of nano-emulsions (NEs) *via* spontaneous emulsification. Our observation reveals the absence of correlation between particle size and physicochemical properties. Instead, particle size appears to be correlated only with the chemical structure of the oils, where the oil with the lower molecular weight (VEA) produces smaller sizes. Thus, the physicochemical mechanisms underlying droplet size formation during spontaneous emulsification remain unclear, highlighting the need for further fundamental research in this field.[66] In addition, the size gradually changes along the composition of the oil mixtures, as seen in Fig. 4(a) and (b). We can note the regular monodispersity along the different formulations, with PDI generally below 0.3. This result demonstrates that altering the oil composition leads to variations in the efficiency of the spontaneous emulsification process, resulting in differences in the size of the nano-emulsion droplets. The relationship between droplet size and the nature of the oil has been documented in the literature[64] and is attributed to the varying affinities of the surfactant for different oils. In this study, we examine the transition between these two compositions. Notably, this transition is not necessarily gradual (*e.g.*, Fig. 4(a)), suggesting that one of the oils, castor oil, dominates the other, leading to a plateau.

3.3.2. Microviscosity measurements in nano-emulsions. Hereafter we compare the viscosities of oil mixtures in cuvettes, with the microviscosity of the nano-emulsion droplets' core. Thus, nano-emulsions encapsulating rBDP-Toco were formulated, with different viscosities –according to the two oil mixtures at different ratios. In this part, our objective was to measure the microviscosity of oil when incorporated into nano-emulsions and to compare it to one of the pure oils or oil mixtures used for their formulation—determining whether the nano-formulation modifies its value. The fluorescence

lifetime was chosen to avoid solubility and concentration issues (as compared to fluorescence intensity values). To this end, values of fluorescence lifetime were compared to the master curve established above in Fig. 3, which is reported in Fig. 5, where two different surfactant amounts –and size ranges– are compared. Fig. 5(a) shows larger nano-emulsions (made with the lower surfactant amount, SOR = 50%) and Fig. 5(b) shows smaller nano-emulsions (made with the higher surfactant amount, SOR = 70%). It is noteworthy that we assume

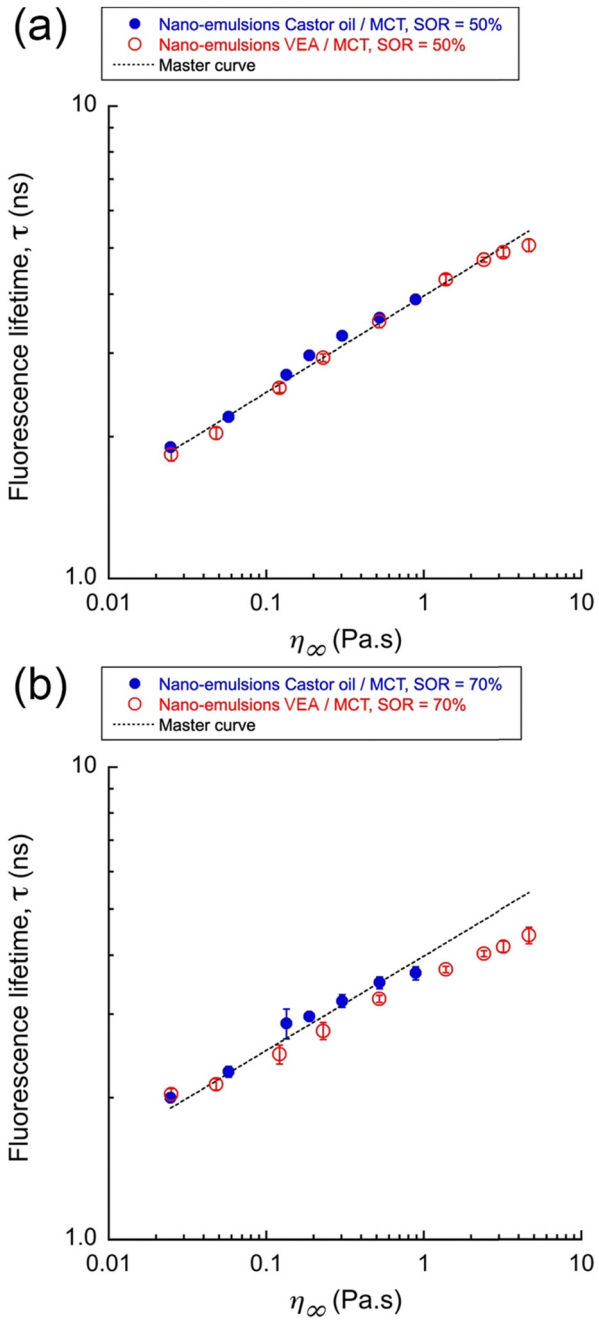

Fig. 5 τ of nano-emulsions made with different oil mixtures (detailed in the legend), as a function of the viscosities (η_∞) of the corresponding oil mixtures composing their core (from Fig. 1). (a) SOR = 50% and (b) SOR = 70%.

rBDP-Toco is fully localized in the droplet core and not partitioned between the core and the interface. Although we cannot determine its exact location, such a configuration would likely result in changes in optical properties, leading to multiple fluorescence peaks and/or different values of the fluorescence lifetime, which are not observed. Furthermore, it seems unlikely that rBDP-Toco exhibits significant amphiphilic properties capable of adsorbing at the interface in competition with the nonionic surfactant used in the formulation.

Two behaviors are revealed: (i) the exact superimposition of the experimental point and the master curve for SOR 50% nano-emulsions, and (ii) the slight shifting between the two curves for SOR 70% nano-emulsions. In case (i) we can deduce an exact correspondence between the viscosities of pure oil and oil in the core of the nano-droplets, whereas, in the case (ii), the slight shift is due to a difference between their viscosities possibly linked to the modification of the composition of the dye environment (as discussed below). It is worth noting that droplet size does not affect the optical properties of the molecular rotor. Fig. 4 shows that an increase in castor oil leads to larger droplet sizes, whereas higher VAE concentrations result in smaller droplet sizes. In contrast, Fig. 5 indicates that the observed effects are independent of droplet size and are instead solely influenced by viscosity.

3.3.3. Quantifying the impact of surfactants on the microviscosity in nano-emulsions. In order to investigate in detail this difference, Fig. 6 reports the comparison of the microviscosities of nano-emulsion droplets denoted by η_{app} (and calculated from the master curve with τ), with the ones of pure oils (η_∞). This comparison appears linear, with the slope s, giving an idea of the real microviscosity of the oil within the nano-droplets, which appears to be decreased compared to pure oil mixtures.

In the case of castor oil/MCT mixtures (Fig. 6(a)), nano-emulsion droplet's core shows a microviscosity very similar whatever the SOR value, with a slope s = 0.88. It follows therefrom that nano-formulation would have a microviscosity of around 90% of the one of the oil mixture, and this difference would be the direct consequence of its intrinsic composition, including a part of the surfactants remaining mixed with oil in the droplets' core. Indicated by the arrow in the figure, nano-emulsions formulated with pure castor oil were remarkably deviated from the general trend, suggesting a viscosity reduced compared to the one of pure oil expected.

As regards the VEA/MCT mixture, a clear difference between the two types of nano-emulsions was revealed, with a slope s = 0.93 for SOR = 50% that reaches a value of s = 0.35 for SOR = 70%. This result signifies that increasing the surfactant amount results in a significant drop in the droplets' core microviscosity of around 35% of the initial value of pure oil mixture –and whatever the ratio of VEA/MCT. This decrease occurs in specific conditions, particularly when using VEA and large surfactant amounts. Therefore, it can be explained by the presence of nonionic surfactants in the oil core of the droplets, which impacts its composition, size and viscosity. This result pertains to a specific case of SOR = 70%, involving

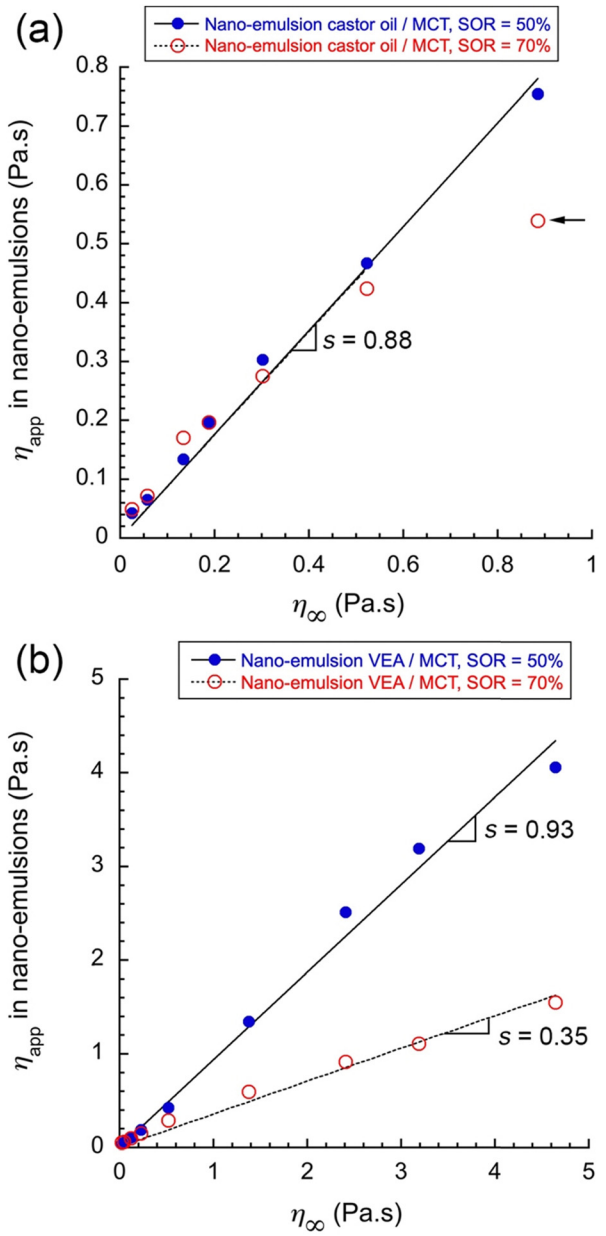

Fig. 6 Comparison of viscosities between oil mixture in the core of nano-emulsion droplets (η_{app}) and pure oil mixtures (η_∞), for two different SOR (SOR = 50% and 70%), and for two different compositions of oil mixtures: castor oil/MCT (a), and VEA/MCT (b). Linear extrapolation and related slopes (*s*) are indicated in the figures (excluding nano-emulsions formulated with pure castor (arrow in (a))).

nano-emulsions formulated with VEA/MCT. In this scenario, the apparent microviscosity (η_{app}) of the nano-emulsion is significantly lower than that of the pure oil mixture. We hypothesize that this difference is due to a modification of the oil composition caused by the surfactants.

Notably, these results do not seem to be correlated with the changes in droplet size shown in Fig. 4. For example, at SOR = 50%, nano-emulsions formulated with VEA/MCT mixtures experienced a significant reduction in droplet size, yet. τ remains comparable to the behavior observed in the cuvette.

When SOR = 50%, the surfactant amount is not sufficient to impact the core properties, which appears similar to the corresponding oil phase –around 93% of the native viscosity –and when SOR = 70% it appears significant enough to impact the oil composition. In contrast, this phenomenon is not observed with the castor oil/MCT mixture, even at the highest surfactant concentration. In this case, it can be assumed that the surfactant is not solubilized within the droplets' core. Specifically, for SOR = 70%, nano-emulsions prepared with castor oil/MCT exhibit an apparent microviscosity η_{app} comparable to the viscosity of the corresponding pure oil mixture. This suggests that the oil composition in the nano-emulsions and in bulk remains similar.

One possible explanation is a change in the composition of the oil droplets due to the integration of surfactants into the oil core of the nano-emulsion droplets. Since this difference is observed when comparing castor oil and VEA, it can be concluded that it depends on the nature of the oil and, consequently, on the affinity between the oil and the surfactant.

In order to investigate the role of nonionic surfactants in the change in the viscosity, and to understand the limits of our hypothesis, we selected the limit case of pure VEA, and we measured fluorescence lifetime of rBDP-Toco in mixtures of VEA with different amounts of nonionic surfactants. In this experiment, we only focused on VEA/surfactant mixtures without water. The results are reported in Fig. 7, presenting the viscosity η_∞ as a function of the composition (Fig. 7(a)) and τ plotted against the viscosity η_∞ (Fig. 7(b)).

The first important result (in Fig. 7(a)) is a significant decrease of η_∞ when adding surfactants. That would corroborate the trend observed in Fig. 6 with nano-emulsions (VEA, SOR = 70%), and our hypothesis to attribute the decrease of lifetime to the viscosity decrease induced by the modification of the droplet composition. However, in Fig. 7(b), the correlation between fluorescence lifetime and viscosity appears not to follow the master curve established with the oil phases, but another behavior resulting from the presence of nonionic surfactants. Fluorescence lifetime decreases much faster compared to the master curve.

In contrast with the former experiment with simple oil mixtures, the surfactant/oil mixture is a fundamentally different system, and this experiment was, indeed, conducted to verify our assumption regarding the change of viscosity induced by a potential integration of surfactants in the oil core of emulsion. Nevertheless, in the case of nano-emulsions made with VEA as oil, and for SOR = 70% (see Fig. 5(b) above), τ = (4.4 ± 0.2) ns. In that case, considering our hypothesis –that the decrease of the fluorescence lifetime can be due to integration of surfactants in oil –the viscosity of the nano-emulsions η_∞^{NE} can be evaluated from fitting exponential function (Fig. 7(b)) as

$$\tau = K_1 + K_2 \cdot e^{\left(\frac{\eta_\infty}{K_3}\right)}$$

in which K_1 = 2.19 ns, K_1 = 0.25 ns and K_3 = 1.79 Pa s are fitting constants. Finally, giving η_∞^{NE} = 3.89 Pa s. From the

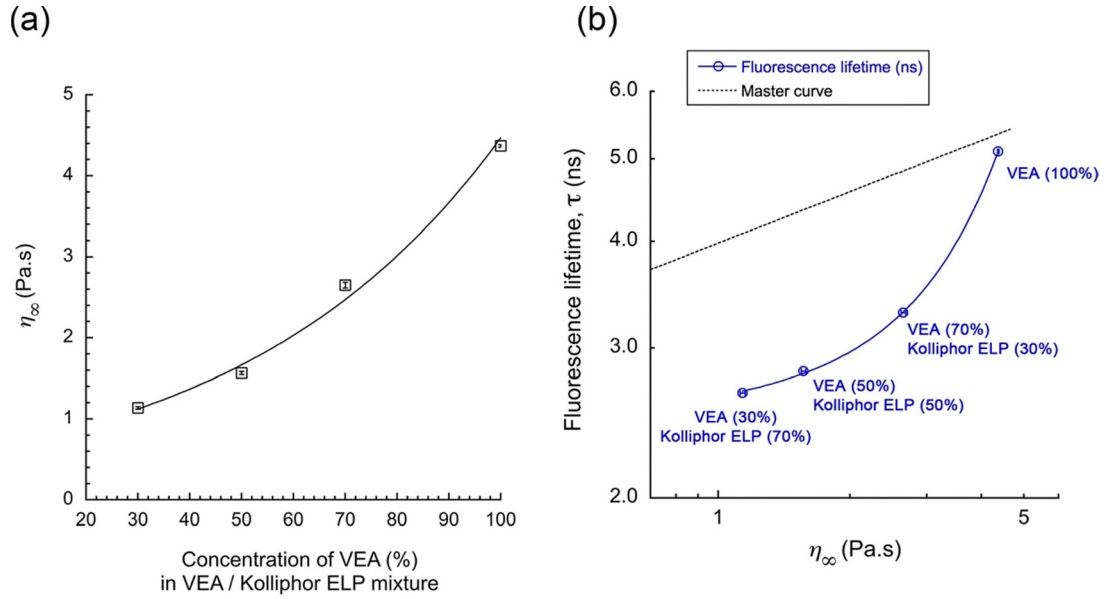

Fig. 7 Characterization of the mixture VEA/Kolliphor ELP (nonionic surfactant). (a) Viscosity for different compositions, and (b) τ of rBDP-Toco as a function of the viscosity, in these VEA/Kolliphor ELP mixtures (where the composition is indicated as labels in the graph). The comparison with the master curve obtained with oil mixtures is also reported in the figure.

extrapolation of the results given in Fig. 7(a),

$$\eta_\infty = K_4 + K_5 \cdot e^{\left(\frac{[\mathrm{VEA}]}{K_6}\right)}$$

in which $K_4 = -0.79$ Pa s, $K_5 = 1.21$ Pa s and $K_6 = 0.014\%$ are fitting constants. This result gives the composition of 91.8% of VEA and 8.2% of Kolliphor ELP, in the nano-emulsion core. Considering the SOR of 70% in the composition of the nano-emulsion, one can note that such a proportion seems nevertheless low, with a significant impact on the viscosity. It is possible that the presence of surfactants brings water molecules. However, as discussed above, these lipophilic molecular rotors are not sensitive to the polarity of their solubilizing medium, and a modification of their solubility does not affect the value of the fluorescence lifetime. Therefore, we should not see the impact of water on the measurement of viscosity. It is worth noting that, although rotors are not sensitive to the polarity, it is possible that viscosity is not the sole parameter influencing their behavior. When used in mixtures of different types, rotors may also exhibit a slight sensitivity to the chemical nature of the components, in addition to the effect of viscosity.

To summarize, molecular rotors allow measuring the micro-viscosities in the nano-emulsion droplets cores –when calibration is done in a similar environment– and can reveal changes due to a modification of their composition. For very high surfactant concentrations, amphiphilic molecules can be incorporated in the oil core and impact on the photophysical properties of the BODIPY rotor. Therefore, the lifetime/viscosity calibration should be carefully adapted to this specific system. It also shows that the nonionic surfactant used in the formulation has a better and specific affinity for VEA compared to MCT and castor oil. Interestingly, this result highlights the strong correlation between the oil/surfactant affinity and the efficiency of the nano-emulsification process; as the droplet's size in function of the composition (Fig. 4) is much more efficient with using VEA.

In this first series of experiments, the master curve showed a correlation between the τ and oil viscosities –regardless of the composition of oil. On the other hand, fluorescence intensities were comparable between the two different oil mixtures –castor oil/MCT and VEA/MCT. Therefore, the results of fluorescence lifetime and fluorescence intensities are significantly different. In general, this difference is attributed to the difference in solubilities of the rotor rBDP-Toco in the oil phase, which exclude the use of FI as a criterion to assess the values of viscosity. Nevertheless, as the composition of oil is also changed with the nano-emulsion formulations, it remains interesting to study the values of FI of nano-emulsion droplets, compared to pure oils. These results are reported in Fig. 8, comparing the two oil mixtures.

In the same way as the results of Fig. 2(b), in which the FI of two oil blends were compared, those of the nano-emulsion formulations appear very similar, even though the viscosity ranges are significantly different. The main remarkable observation lies in the fact that nano-emulsions present a higher brightness when oil is formulated compared to pure oil. In addition, FI increases when SOR increases, one can see the FI increases when the viscosity increases, but also that both (i) the nano-emulsification and (ii) the size of the droplets, have a significant impact on the fluorescence intensity. The correlation between FI and size could be due to the slight modification of the oil composition when the presence of surfactants is gradually increased in the nano-emulsion oil core. It confirms

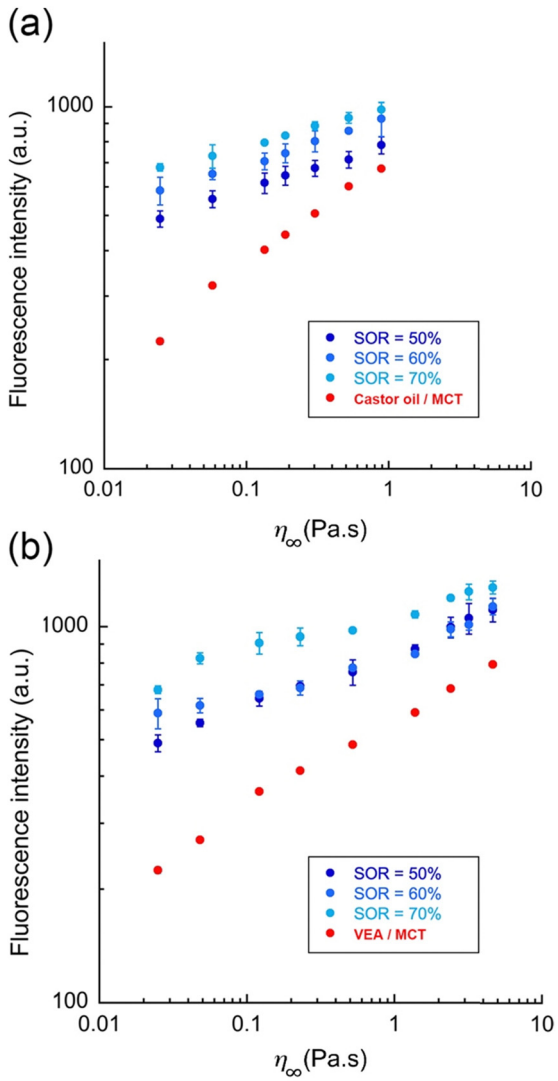

Fig. 8 FI of oil mixtures and their respective nano-emulsions formulations in function of the viscosities (η_∞) of the different oil mixtures: (a) castor oil/MCT and (b) VEA/MCT. Different nano-emulsion size range was compared to each other and compared with pure oil mixture. FI intensity was normalized to the oil amounts in the formulations.

that fluorescent lifetime measurements are much more adapted in our case to measure viscosity with molecular rotors. We hypothesize that this result is directly related to the impact of dye solubility, increased by surfactants when oil is formulated as in the form of nano-emulsions. As a result, FI is drastically increased.

4. Conclusion

In this study, we synthesized a lipophilic fluorescent viscosity probe based on BODIPY, namely rBDP-Toco, through the coupling of a well-established molecular rotor with tocopherol. rBDP-Toco was then used to sense the viscosity of the oil core in nano-formulations such as nano-emulsions.

To date, microviscosity in colloidal systems is mostly measured using nanoparticles tracking, and monitoring –for instance– their magnetic properties,[16] or tracking their mobility.[17] These approaches are powerful, but are limited by the size of these nanoparticles. On the other hand, molecular rotors are known to be efficient as sensors of microenvironments, and particularly lipophilic BODIPY rotors are recognized as viscosity sensor with a weak sensitivity to polarity.[1,46,50]

We showed this experimental approach is efficient to sense the viscosity of lipid nano-dispersion like nano-emulsion, and can also reveal specific modifications of the droplet composition, like evidence of integration of surfactants in the composition of the oil core. The comprehensive optical calibration in oil mixtures with different viscosities was assessed and gave the correlation between the fluorescence intensity, the fluorescence lifetime, and the dynamic viscosity. It allows showing a universal behavior between viscosity and fluorescent lifetime, at constant temperature regardless of the composition of the oil phase. This calibration was then applied to different types of nano-emulsions encapsulating rBDP-Toco. Thus, our main result lies in the possibility to sense the microviscosity of the nano-droplets' oil core, independently of their size and composition. In comparison with literature, mainly devoted to the use of molecular rotors for very specific targets and generally hydrophilic domains,[13–15] here we propose a calibration in lipid medium, and an original application to sense the properties of lipid nano-domains. This approach could also be applied to generate nano-emulsions with specific microviscosity by measuring and adjusting it at a macroscopic scale (through the choice of oil and SOR), and subsequently verifying the droplets' core viscosity after formulation.

This approach allows disclosing slight variation of the oil viscosities, likely due to the presence of nonionic surfactants that remain solubilized in the oil core. A deeper characterization of the oil/surfactant mixture revealed the potential of this approach to understand the composition of the nano-droplets. An extension of these findings could involve utilizing a series of molecular rotors to map the observed variations in viscosity within a given lipophilic medium, as monitored through fluorescence lifetime imaging microscopy (FLIM). In this work, we present evidence supporting the concept of viscosity sensing inside droplets at the nanometric scale and demonstrate that slight modifications in the observed viscosities can reveal notable differences in the interactions between the compounds used in the formulation.

Data availability

The data supporting this article have been included as part of the ESI.†

Conflicts of interest

There are no conflicts to declare.

Acknowledgements

M. E. acknowledges the Pierre Fabre Foundation for financial support.

References

1 A. Vyšniauskas, I. López-Duarte, N. Duchemin, T.-T. Vu, Y. Wu, E. M. Budynina, Y. A. Volkova, E. Peña Cabrera, D. E. Ramírez-Ornelas and M. K. Kuimova, *Phys. Chem. Chem. Phys.*, 2017, **19**, 25252–25259.
2 M. K. Kuimova, *Phys. Chem. Chem. Phys.*, 2012, **14**, 12671.
3 X. Qin, X. Yang, L. Du and M. Li, *RSC Med. Chem.*, 2021, **12**, 1826–1838.
4 E. Xochitiotzi-Flores, A. Jiménez-Sánchez, H. García-Ortega, N. Sánchez-Puig, M. Romero-Ávila, R. Santillan and N. Farfán, *New J. Chem.*, 2016, **40**, 4500–4512.
5 Z. Yang, J. Cao, Y. He, J. H. Yang, T. Kim, X. Peng and J. S. Kim, *Chem. Soc. Rev.*, 2014, **43**, 4563–4601.
6 J. M. Nölle, C. Jüngst, A. Zumbusch and D. Wöll, *Polym. Chem.*, 2014, **5**, 2700–2703.
7 A. Athanasiadis, C. Fitzgerald, N. M. Davidson, C. Giorio, S. W. Botchway, A. D. Ward, M. Kalberer, F. D. Pope and M. K. Kuimova, *Phys. Chem. Chem. Phys.*, 2016, **18**, 30385–30393.
8 M. Paez-Perez and M. K. Kuimova, *Angew Chem., Int. Ed.*, 2024, **63**, e202311233.
9 A. Vyšniauskas, M. Qurashi and M. K. Kuimova, *Chem. - Eur. J.*, 2016, **22**, 13210–13217.
10 M. R. Dent, I. López-Duarte, C. J. Dickson, N. D. Geoghegan, J. M. Cooper, I. R. Gould, R. Krams, J. A. Bull, N. J. Brooks and M. K. Kuimova, *Phys. Chem. Chem. Phys.*, 2015, **17**, 18393–18402.
11 E. Gatzogiannis, Z. Chen, L. Wei, R. Wombacher, Y.-T. Kao, G. Yefremov, V. W. Cornish and W. Min, *Chem. Commun.*, 2012, **48**, 8694.
12 X. Peng, Z. Yang, J. Wang, J. Fan, Y. He, F. Song, B. Wang, S. Sun, J. Qu, J. Qi and M. Yan, *J. Am. Chem. Soc.*, 2011, **133**, 6626–6635.
13 A. Vyšniauskas and M. K. Kuimova, *Int. Rev. Phys. Chem.*, 2018, **37**, 259–285.
14 S. Toliautas, J. Dodonova, A. Žvirblis, I. Čiplys, A. Polita, A. Devižis, S. Tumkevičius, J. Šulskus and A. Vyšniauskas, *Chem. - Eur. J.*, 2019, **25**, 10342–10349.
15 L. Michels, V. Gorelova, Y. Harnvanichvech, J. W. Borst, B. Albada, D. Weijers and J. Sprakel, *Proc. Natl. Acad. Sci. U. S. A.*, 2020, **117**, 18110–18118.
16 R. R. Merchant, L. Maldonado-Camargo and C. Rinaldi, *J. Colloid Interface Sci.*, 2017, **486**, 241–248.
17 T. Moschakis, A. Lazaridou and C. G. Biliaderis, *J. Colloid Interface Sci.*, 2012, **375**, 50–59.
18 K. I. Momot and P. W. Kuchel, *Concepts Magn. Reson., Part A*, 2003, **19A**, 51–64.
19 E. V. Morozov, P. V. Nizovtseva and O. N. Martyanov, *Energy Fuels*, 2022, **36**, 14696–14709.
20 B. Medronho, A. Filipe, C. Costa, A. Romano, B. Lindman, H. Edlund and M. Norgren, *J. Colloid Interface Sci.*, 2018, **531**, 225–232.
21 X. Li, J. van der Gucht, P. Erni and R. de Vries, *J. Colloid Interface Sci.*, 2023, **632**, 357–366.
22 S. O. Raja, G. Sivaraman, S. Biswas, G. Singh, F. Kalim, P. Kandaswamy and A. Gulyani, *ACS Appl. Bio Mater.*, 2021, **4**, 4361–4372.
23 X. Wu and C. Barner-Kowollik, *Chem. Sci.*, 2023, **14**, 12815–12849.
24 M. Y. Berezin and S. Achilefu, *Chem. Rev.*, 2010, **110**, 2641–2684.
25 A. Polita, S. Toliautas, R. Žvirblis and A. Vyšniauskas, *Phys. Chem. Chem. Phys.*, 2020, **22**, 8296–8303.
26 T. T. Vu, R. Méallet-Renault, G. Clavier, B. A. Trofimov and M. K. Kuimova, *J. Mater. Chem. C*, 2016, **4**, 2828–2833.
27 T. F. Vandamme, *Int. J. Pharm.*, 2009, **377**, 142–147.
28 M. Yao, H. Xiao and D. J. McClements, *Annu. Rev. Food Sci. Technol.*, 2014, **5**, 53–81.
29 V. K. Rai, N. Mishra, K. S. Yadav and N. P. Yadav, *J. Controlled Release*, 2018, **270**, 203–225.
30 M. Kah and T. Hofmann, *Environ. Int.*, 2014, **63**, 224–235.
31 Ş. Yalçınöz and E. Erçelebi, *Mater. Res. Express*, 2018, **5**, 062001.
32 M. N. Yukuyama, D. D. M. Ghisleni, T. J. A. Pinto and N. A. Bou-Chacra, *Int. J. Cosmet. Sci.*, 2016, **38**, 13–24.
33 A. S. Klymchenko, F. Liu, M. Collot and N. Anton, *Adv. Healthcare Mater.*, 2021, **10**, 2001289.
34 X. Li, N. Anton, G. Zuber and T. Vandamme, *Adv. Drug Delivery Rev.*, 2014, **76**, 116–133.
35 N. Anton, F. Hallouard, M. F. Attia and T. F. Vandamme, in *Intracellular Delivery III*, ed. A. Prokop and V. Weissig, Springer International Publishing, Cham, 2016, pp. 273–300.
36 A. S. Klymchenko, E. Roger, N. Anton, H. Anton, I. Shulov, J. Vermot, Y. Mely and T. F. Vandamme, *RSC Adv.*, 2012, **2**, 11876.
37 V. N. Kilin, H. Anton, N. Anton, E. Steed, J. Vermot, T. F. Vandamme, Y. Mely and A. S. Klymchenko, *Biomaterials*, 2014, **35**, 4950–4957.
38 X. Wang, N. Anton, P. Ashokkumar, H. Anton, T. K. Fam, T. Vandamme, A. S. Klymchenko and M. Collot, *ACS Appl. Mater. Interfaces*, 2019, **11**, 13079–13090.
39 N. Anton, S. Akram and T. F. Vandamme, in *Nanoemulsions*, ed. S. M. Jafari and D. J. McClements, Academic Press, 2018, pp. 77–100.
40 N. Anton and T. F. Vandamme, *Int. J. Pharm.*, 2009, **377**, 142–147.
41 X. Ma, R. Sun, J. Cheng, J. Liu, F. Gou, H. Xiang and X. Zhou, *J. Chem. Educ.*, 2016, **93**, 345–350.
42 A. Mushtaq, S. Mohd Wani, A. R. Malik, A. Gull, S. Ramniwas, G. Ahmad Nayik, S. Ercisli, R. Alina Marc, R. Ullah and A. Bari, *Food Chem.:X*, 2023, **18**, 100684.
43 D. Myers, Liquid-fluid interfaces, in *Surfaces, Interfaces, and Colloids*, ed. D. Myers, John Wiley & Sons, Ltd, 2002, ch. 8, pp. 140–178.
44 W. D. Bancroft, *J. Phys. Chem.*, 1913, **17**, 501–519.
45 W. Miao, C. Yu, E. Hao and L. Jiao, *Front. Chem.*, 2019, **7**, 825.
46 X. Wang, S. Bou, A. S. Klymchenko, N. Anton and M. Collot, *Nanomaterials*, 2021, **3**, 826–838.

47 P. Ashokkumar, A. H. Ashoka, M. Collot, A. Das and A. S. Klymchenko, *Chem. Commun.*, 2019, **55**, 6902–6905.
48 K. T. Fam, L. Saladin, A. S. Klymchenko and M. Collot, *Chem. Commun.*, 2021, **57**, 4807–4810.
49 Y. Wu, M. Štefl, A. Olzyńska, M. Hof, G. Yahioglu, P. Yip, D. R. Casey, O. Ces, J. Humpolíčková and M. K. Kuimova, *Phys. Chem. Chem. Phys.*, 2013, **15**, 14986–14993.
50 J. A. Levitt, P.-H. Chung, M. K. Kuimova, G. Yahioglu, Y. Wang, J. Qu and K. Suhling, *ChemPhysChem*, 2011, **12**, 662–672.
51 M. R. Bittermann, M. Grzelka, S. Woutersen, A. M. Brouwer and D. Bonn, *J. Phys. Chem. Lett.*, 2021, **12**, 3182–3186.
52 D. Zhu, M. A. Haidekker, J.-S. Lee, Y.-Y. Won and J. C.-M. Lee, *Macromolecules*, 2007, **40**, 7730–7732.
53 A. Polita, M. Stancikaitė, R. Žvirblis, K. Maleckaitė, J. Dodonova-Vaitkūnienė, S. Tumkevičius, A. P. Shivabalan and G. Valinčius, *RSC Adv.*, 2023, **13**, 19257–19264.
54 D. Su, C. L. Teoh, N. Gao, Q.-H. Xu and Y.-T. Chang, *Sensors*, 2016, **9**, 1397–1406.
55 A. Vyšniauskas, M. Qurashi, N. Gallop, M. Balaz, H. L. Anderson and M. K. Kuimova, *Chem. Sci.*, 2015, **6**, 5773–5778.
56 A. U. Rehman, *Eur. J. Pharm. Res.*, 2019, **1**, 27–36.
57 S. Ding, B. Mustafa, N. Anton, C. A. Serra, D. Chan-Seng and T. F. Vandamme, *Int. J. Pharm.*, 2020, **585**, 119481.
58 J. Stetefeld, S. A. McKenna and T. R. Patel, *Biophys. Rev.*, 2016, **8**, 409–427.
59 M. Zhang, Y. Yang and N. C. Acevedo, *Food Biophys.*, 2020, **15**, 473–481.
60 T. Förster and G. Hoffmann, *Z. Phys. Chem.*, 1971, **75**, 63–76.
61 R. O. Loutfy and B. A. Arnold, *J. Phys. Chem.*, 1982, **86**, 4205–4211.
62 S. Akram, N. Anton, Z. Omran and T. Vandamme, *Pharmaceutics*, 2021, **13**, 1030.
63 X. Wang, M. Collot, T. F. Vandamme and N. Anton, *Colloids Surf., A*, 2022, **645**, 128858.
64 M. F. Attia, N. Anton, R. Akasov, M. Chiper, E. Markvicheva and T. F. Vandamme, *Pharm. Res.*, 2016, **33**, 603–614.
65 M. F. Attia, N. Anton, M. Chiper, R. Akasov, H. Anton, N. Messaddeq, S. Fournel, A. S. Klymchenko, Y. Mély and T. F. Vandamme, *ACS Nano*, 2014, **8**, 10537–10550.
66 A. H. Saberi, Y. Fang and D. J. McClements, *J. Colloid Interface Sci.*, 2013, **391**, 95–102.